International Journal of GEOMATE, Aug., 2024 Vol.27, Issue 120, pp.1-8
ISSN: 2186-2982 (P), 2186-2990 (O), Japan, DOI: https://doi.org/10.21660/2024.120.g13252
Geotechnique, Construction Materials and Environment

A NUMERICAL SIMULATION OF LOCAL SCOUR PROCESS DUE TO WAVES AROUND MONOPILE FOUNDATION USING REEF3D

*Tatsuya Matsuda[1], Kinya Miura[1], Naoto Naito[1] and Daiki Shirakura[1]

[1] Department of Architecture and Civil Engineering, Toyohashi University of Technology, Japan

*Corresponding Author, Received: 18 June 2023, Revised: 14 Mar. 2024, Accepted: 29 May 2024

ABSTRACT: Monopile foundations are commonly constructed for offshore wind turbines and installed at depths shallower than 30 m. However, preventing scouring and erosion around the pile foundation due to waves is critical, as this can cause instability of the foundations and supported structures. In this study, model and numerical tests were conducted to investigate wave-induced scour and erosion around a monopile foundation and clarify the fundamental mechanisms involved. Numerical tests were conducted and validated against physical model tests for a bare sea bed, and good reproducibility was obtained. When a monopile foundation was installed in both the numerical and physical tests, the flow velocity on the seabed in the offshore and inshore directions increased on the side of the foundation perpendicular to the direction of the wave motion. In the model test, scouring occurred at the same location, indicating that scouring may have been caused by the flow velocity; however, this scouring occurred locally, suggesting the need for a detailed analysis of the associated factors.

Keywords: Sea wave, Offshore wind turbine, Monopole, Scour, Model test, REEF3D

1. INTRODUCTION

Monopile foundations have superior workability and economic efficiency compared to other foundations and are among those used for offshore wind power. They are actively being used in Europe, where there is currently significant offshore wind power development. However, the applicability of monopile foundations to complex seabed conditions, such as those in Japan, where soft ground and bedrock are mixed, has not been fully investigated. There is also a need for further research into their stability against natural external forces such as seismic motions, tsunamis, storm surges, and high waves caused by typhoons and low-pressure systems. Therefore, studies of the stability of monopile foundations are being actively conducted to introduce them in Japan.

Scouring in monopile foundations due to wave and current are of particular concern. For the development of effective scouring countermeasures, it is necessary to analyze the effects of external wave forces on sandy soil and thus evaluate the stability of monopile foundation structures.

A previous study on scouring around upright cylindrical structures caused by waves focused on the maximum scour depth and final scour profile (Summer et al., 1992 [1]). Based on the results of a series of model experiments, Summer et al. proposed a formula for estimating the maximum scour depth according to the KC number. Recently, more specific studies have been conducted on the stability of the monopile foundations of wind turbines (Mayall et al., 2018 [2]; Miyamoto et al., 2018 [3]). Miyamoto et al. (2018) used a centrifuge model test to show that the process of wave-induced liquefaction is progressive. Matsuda et al. (2021) [4] investigated the scouring process around a cylindrical structure by considering the shear stress on the seabed surface and the effective stress response of the seabed. Their results showed that excess pore water pressure in the seabed was generated by waves and that the change in the effective stress response of the seabed differed between locations around the structure. They also found that the seabed on the sides of the cylindrical structure was clearly scoured. These findings indicate a requirement for measures to be implemented to prevent the scouring and seabed instability caused by waves around cylindrical structures. In previous studies [1]-[4], wave characteristics and sediment dynamics around cylindrical structures have been investigated through movable-bed experiments using wave flume channels. However, the limitations and costs of model-based tests, such as equipment and facilities, limit the number of cases that can be studied.

The object of this study is to clarify the wave-induced scour process around cylindrical structures considering the characteristics of geomaterials. In this study, numerical simulations using REEF3D (Kamath et al., 2015 [5]; Ahmad et al., 2018 [6]) were conducted to understand the detailed wave characteristics around a cylindrical structure and analyze the effect of the wave response at the bottom boundary on sediment dynamics. The reproducibility of the wave response around with and without the installation of the cylindrical structure was verified in a fixed-bed experiment using a wave flume channel. Based on the numerical results of the wave response, sediment transport phenomena were predicted by comparing the topographic changes observed in the model test with the wave response around the cylindrical structure.

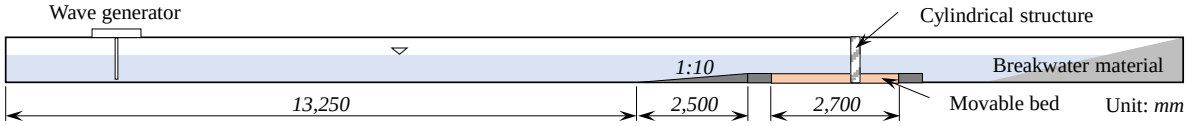

Fig.1 Schematic of a wave flume channel

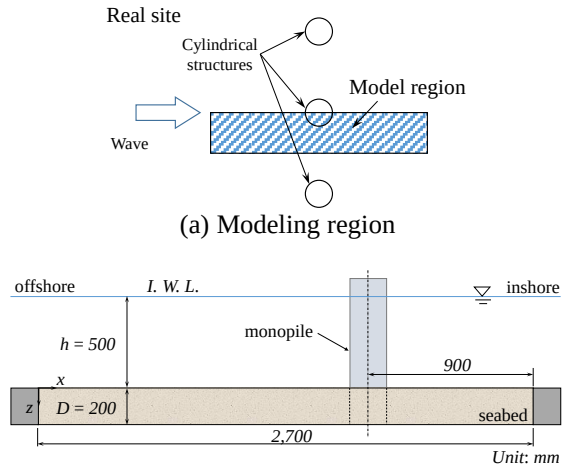

Fig.2 Modeling region of movable bed in a model experiment

2. RESEARCH SIGNIFICANCE

In this study, REEF3D is performed to reproduce the wave field of the model experiment and to verify that the discus to wave response is reproduced with high accuracy. In addition, a qualitative evaluation of wave-induced sediment transport phenomena is conducted by comparison with model experiments. REEF3D will be able to predict the scouring process around cylindrical structures considering the geomaterial characteristics, which is the objective of this study because a sediment transport model is introduced in REEF3D. This study will also be useful for elucidating sediment dynamics around monopile foundations in wave fields and for studying countermeasure methods.

3. METHODS AND MATERIALS

3.1 Experimental Method

Fig. 1 shows a schematic of the wave flume channel, which was 25 m long, 0.6 m wide, and 1.0 m high. A movable bed (2.7 m long, 0.6 m wide, and 0.2m high) was installed in the channel. Froude's similarity law was considered when establishing the hydraulic conditions; most model tests in coastal engineering are scaled based on the Froude criterion. The similarity rate was set at λ_L=1/25. Thus, the scale factors of the flow velocity and time were derived as $\lambda_L^{0.5}$. Fig. 2(a) shows the target region of this study, which, as mentioned above, focuses on the transportation of the seabed around cylindrical structures. In particular, this study targeted structures installed at right angles to the incident wave direction at equal intervals. An acrylic half-cylinder set at the side of the channel was used as the model. Figs 2(b) and 2(c) show the model domain of the target region and the positions of the various sensors. During the experiments, the wave level and flow velocity above the sediment area were measured using a capacitive wave gauge and an electromagnetic flow meter. The pore water pressure in the ground was measured using pore water pressure sensors positioned at z = 0.00, 0.025, and 0.05 m below the seabed surface at angles of θ = 0°, 45°, and 90° (in the circumferential direction, relative to the front of the structure). The surface profile of the movable bed was measured using an ultrasonic sensor.

Table 1 Physical properties of geomaterial

	Silica sand #8
Mean diameter, D_{50} (mm)	0.109
Maximum void ratio, e_{max}	1.218
Minimum void ratio, e_{min}	0.670
Coefficient of permeability, k (m/s)	1.41×10^{-5}

Froude's similarity law has limitations when applied to the geometric scaling of geomaterials. This study focused on the transport of fine sand with an average grain size D_{50} of 0.2 mm in a prototype. When applying Froude's similarity law to the prototype using fine sand ($D_{50}|_p$ = 0.2 mm), the required geomaterial for the model sediment was classified as silt ($D_{50}|_m$ = 0.008 mm). Therefore, in this study, the Dean Number (Dean, 1973 [7]) was used to select the geomaterials. This resulted in the selection of very fine sand for the model sediment ($D_{50}|_m$ = 0.075 mm) when the prototype used fine sand ($D_{50}|_p$ = 0.2 mm). The model experiment used a silica sand #8 which is considering the Dean Number. Table 1 shows the physical properties of silica sand #8.

3.2 Numerical Simulation Method

The governing equations in the REEF3D model are the incompressible Reynolds-Averaged Navier–Stokes equations (RANS equations) and continuity equations.

$$\frac{\partial u_i}{\partial x_i} = 0 \tag{1}$$

$$\frac{\partial u_i}{\partial t} + u_j \frac{\partial u_i}{\partial x_j} = -\frac{\partial P}{\partial x_i} + \frac{\partial}{\partial x_j}\left[\nu\left(\frac{\partial u_i}{\partial x_j} + \frac{\partial u_j}{\partial x_i}\right) - \overline{u_i u_j}\right] + g_i \tag{2}$$

where u: flow velocity, t: time, x: position, v: kinematic viscosity, ρ: density of water, P: pressure, and g: gravity.

Calculations of wave propagation based on the Navier–Stokes equations must be discretized with high accuracy because of the possibility of wave damping. A fifth-order WENO scheme was used as the discretization method for flow velocity. In this scheme, all smooth functions are weighted and averaged to maintain a high accuracy. In particular, the k-ω model was used to calculate turbulent flow, where k and ω are the turbulent kinematic energy and the specific turbulent dissipation, respectively, determining the turbulent scale.

REEF3D, which handles two-phase flows, uses the level-set method to represent the gas–liquid boundary surface. The boundary phase of the two-phase flow was defined as the reference interface, and the inside and outside of the boundary were defined as distance functions.

The sediment transport motions are considered the bedload and suspended load [8]. The bedload is calculated using the van Rijn formula (van Rijin, 1984) [9] that is based on the Shields approach (Shields, 1936) [10]; That is,

$$\frac{q_B}{d_{50}^{1.5}\sqrt{(s-1)g}} = 0.053\frac{T^{2.1}}{D_*^{0.3}} \tag{3}$$

where

$$T = \left(\tau - \tau_{cr}\right)/\tau_{cr} \tag{4}$$

$$D_* = d_{50}\left[\frac{(s-1)g}{\nu^2}\right]^{\frac{1}{3}} \tag{5}$$

Here, τ_{cr} is the modified Shields critical bed shear stress, s is the specific density, v is the kinematic viscosity of water, g is the acceleration gravity, and d_{50} is the median sediment particle diameter.

The suspended sediment load is calculated using the convection-diffusion equation as follows:

$$\frac{\partial c}{\partial t} + u_j \frac{\partial c}{\partial x_j} + w_s \frac{\partial c}{\partial z} = \frac{\partial}{\partial x_j}\left(\Gamma \frac{\partial c}{\partial x_j}\right) \tag{6}$$

where c is the suspended load concentration, Γ is the sediment mixing coefficient, and w_s is the fall velocity of the sediment particles in the water, calculated based on the Stokes law.

The bed level changes are calculated using the Exner formula, which is based on the conservation of the mass of sediments transported by the flow and deposited from suspension. The Exner formula used for bed level change is described as follows:

$$\frac{\partial z_b}{\partial t} + \frac{1}{(1-n)}\left[\frac{\partial q_{B,x}}{\partial x} + \frac{\partial q_{B,y}}{\partial y}\right] + E - D = 0 \tag{7}$$

where q_B is the bed load in each direction, n is porosity, z_b is the bed surface elevation, E is the erosion rate, and D is the corresponding deposition rate from suspended sediments.

4. WAVE PROPAGATION ON FLAT SEABED

This section describes the results of the tests and analyses conducted to examine the reproducibility of the wave field in passing waves. Thus, the test results described here were obtained without including a cylindrical structure on the seabed.

4.1 Numerical Analysis Results

To reproduce the model test's movable bed region, an analysis domain 10 m long, 1.2 m wide, and 1.0 m high was set up in the numerical analysis, and waves were generated from the leftmost boundary of the domain (Fig. 3). The water depth was set to 0.5 m, as in the model test. An attenuation region was established to reduce the effects of waves reflected from the boundary. Based on the results of a preliminary study, a 3.0 m attenuation region from the right edge of the analysis domain was specified.

The results of the numerical analyses are presented in Table 2. In this analysis, the wave heights were set according to two cases. The wave conditions were set as regular waves with period of 1.6 s. The mesh size in the numerical analysis was cubic shape of 0.02 m.

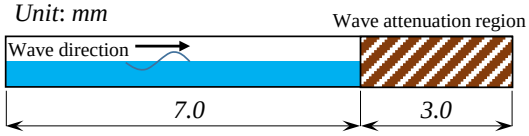

Fig.3 Numerical Analysis domain for the study of wave response on flat seabed

Table 2 Physical properties of geomaterial

	Value
Wave height, H (m)	0.0345
	0.0714
Wave period, T (s)	1.6
Attenuation region length (m)	3.0

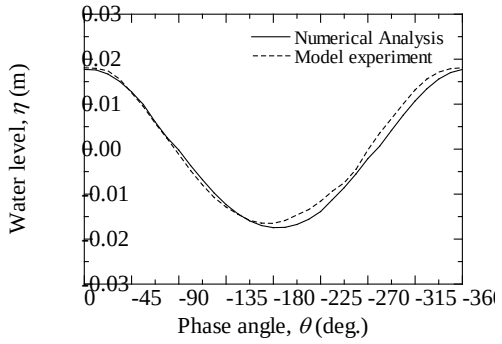

(a)

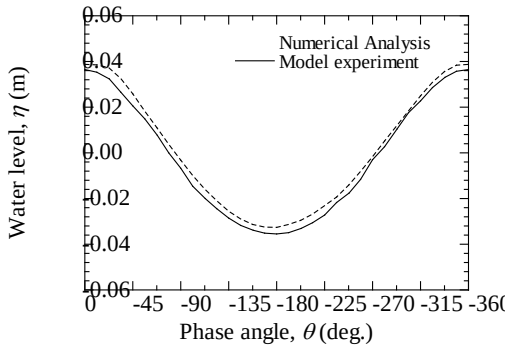

(b)

Fig.4 Comparison of water level fluctuations between model experiment and numerical analysis.

Table 3 Comparison of water height.

Model experiment (m)	Numerical Analysis (m)
0.0345	0.0352
0.0712	0.0720

4.2 Comparison between Numerical and Model Experiment Results

Fluctuations in water level and horizontal velocities without a cylindrical structure in the wave field were compared between the results of the physical model experiments and numerical analyses. For both test types, data from several waves were averaged to represent the change in one cycle as the phase angle, using the averaging method described by Matsuda et al. (2018) [11].

Fig. 4 shows a comparison of water level

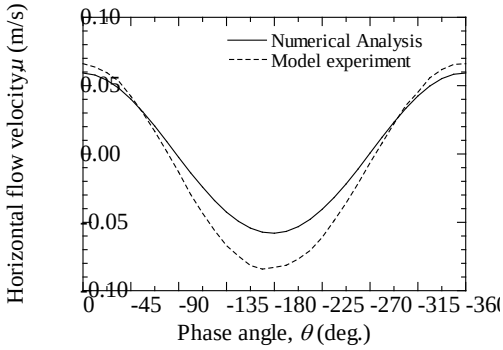

(a)

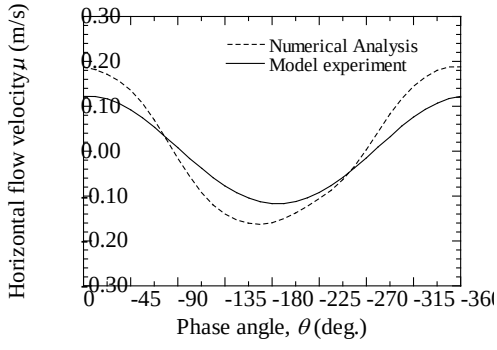

(b)

Fig.5 Comparison of horizontal flow velocity between model experiment and numerical analysis.

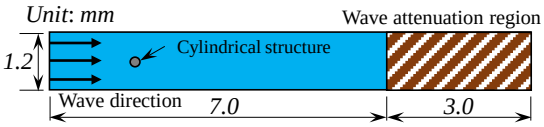

Fig.6 Numerical Analysis domain for the study of prediction of wave response and sediment transport around cylindrical structure

fluctuations. In the numerical analyses, the water level was measured at the center of the installation position of the cylindrical structure, as in the model experiment. The water level fluctuations were generally the same in the numerical analysis and model experiment, regardless of the wave height, confirming the reproducibility of the numerical analysis.

The wave heights are listed in Table 3. An error of only 6.3×10^{-4} m and 6.1×10^{-4} m was observed between simulated and experimental values, indicating that the calculations were highly accurate. Fig. 5 presents a comparison of the horizontal water velocities measured 0.03 m above the seabed surface. The experimentally obtained flow velocities were slightly larger than those of experimental results; however, the results are generally considered valid. The reason for this difference may be the installation conditions of the measuring instruments used in the experiment, or the influence of reflections from the boundary.

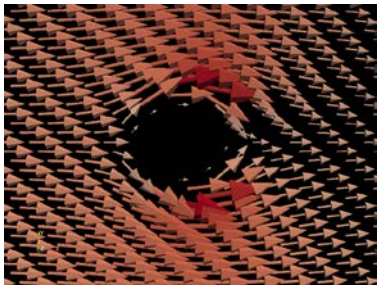

(a) θ = 0°

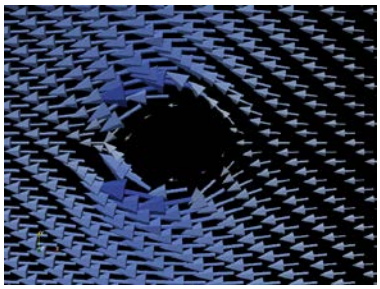

(b) θ = 180°

Fig.7 Numerical analysis results: Horizontal velocity vectors at 1.0×10^{-4} m from the sea bed in the vicinity of the cylindrical structure

5. PREDICTION OF WAVE RESPONSE AND SEDIMENT TRANSPORT AROUND CYLINDRICAL STRUCTURE

In the previous section, we confirmed the reproducibility of the wave field in passing waves without including a cylindrical structure in the numerical analyses or physical experiments. This section describes the results of the wave response analysis conducted with the installation of a cylindrical structure, and discusses the sediment transport obtained in the model experiment.

5.1 Numerical Analysis Results

The numerical analysis conditions were the same as in the previous section, and a semi-cylindrical structure with a diameter of 0.2 m, assuming a monopile foundation, was installed at the location shown in Fig. 6. The external wave force was determined based on the *KC* number, which is expressed by the following equation:

$$KC = \frac{U_m T}{D} \tag{3}$$

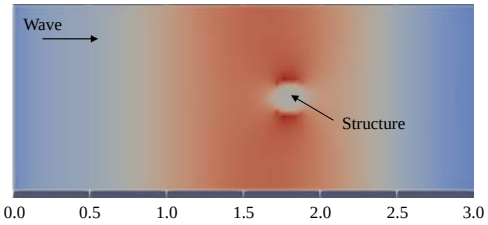

(a) θ = 0°

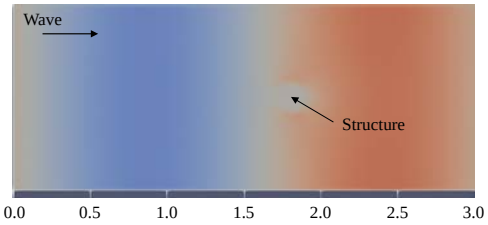

(b) θ = 90°

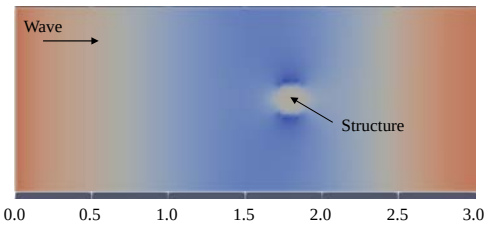

(c) θ = 180°

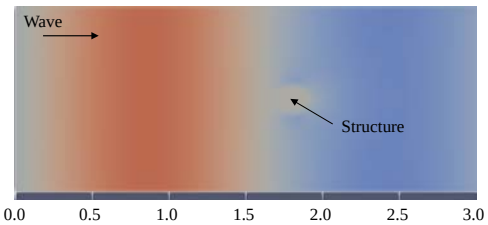

(d) θ = 270°

Fig.8 Numerical analysis results: Planar distribution of *x*-direction velocity contour at 1.0×10^{-4} m from the sea bed.

Here, U_m is the amplitude of the near-bed velocity, T is the wave period and D is a diameter of cylindrical structure.

Because sediment transport was observed in the model experiment when the *KC* number was 0.8, a *KC* number of 0.8 was used in the numerical analysis. Fig. 7 shows the velocity vectors at 1.0×10^{-4} m from the sea bed in the vicinity of the cylindrical structure and Fig. 8 shows the planar distribution of *x*-direction velocity contour at 1.0×10^{-4} m from the sea bed. The wave direction is positive, and the vectors are colored. When the offshore side of the cylinder was 0°, the positive and negative velocity vectors due to waves were large near the sides of the structure (30–135°) in

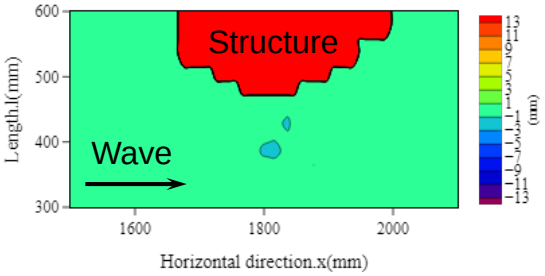

(a) 100 wave loadings

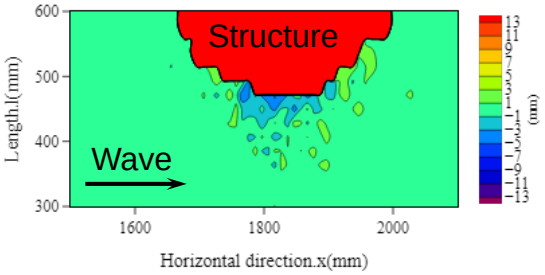

(b) 600 wave loadings

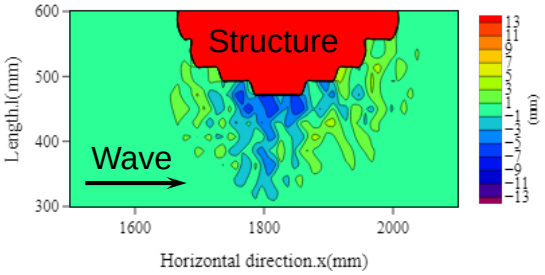

(c) 1200 wave loadings

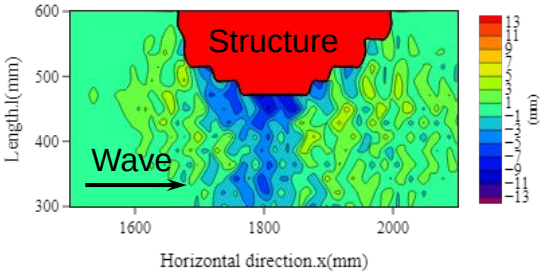

(d) 2400 wave loadings

Fig.9 Model experiment result: Topographic change in the movable bed.

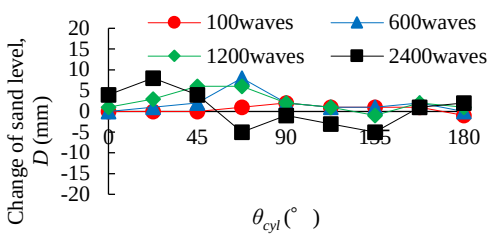

Fig.10 Model experiment results: Changes of bed surface level on the side of the cylindrical structure due to wave.

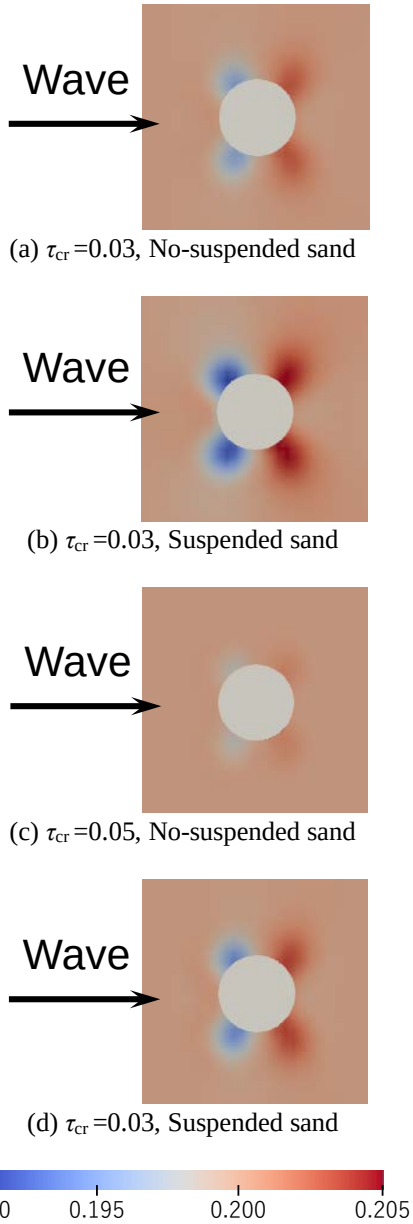

Fig.11 Numerical results: Topographic change in the movable bed after 2400 wave loadings

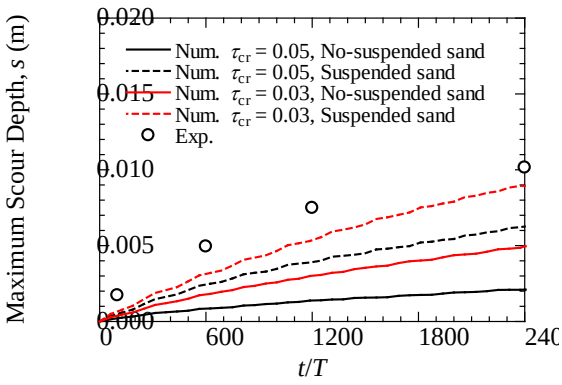

Fig.12 Compared between model experiment and numerical results of maximum scour depth around a cylindrical structure.

Fig. 7. This is considered to have caused localized scouring, as shown in the model test results. The velocities at 0° and 180° were so low that no sediment transport was expected to occur; however, sand transported by the flow along the columnar structure was expected to accumulate in these areas. The diffracted waves generated by the columnar structure cause the flow velocity to increase at approximately 90° along the side of the structure, even at a short distance from the boundary of the columnar structure; thus, the scour is considered to have expanded in the direction normal to the outward direction of the structure boundary at approximately 90° in the model experiment.

5.2 Comparison between Numerical and Model Experiment Results

Fig. 9 shows the topographic changes in the movable bed during the model experiment. With wave loading, ripple-like landforms were observed at θ_{cyl} = 90°. This topographic change formed at θ_{cyl} = 90° later expanded and was observed when 1200 and 2400 waves had been loaded, respectively. Furthermore, scouring progressed in the vertical direction, and the scouring depth increased over time. Fig. 10 shows the changes of bed surface level on the side of the cylindrical structure. The angle was 0° at the channel junction on the offshore side of the cylindrical structure and was positive counterclockwise. A gradual change in the ground surface shape was observed after wave loading. After 2400 waves were loaded, erosion was observed near 90°, and sedimentation was observed at 0° and 180°.

Subsequently, the numerical results are presented. In the numerical simulation, a movable bed with a layer thickness of 0.2 m was set up in the analysis domain shown in Figure 6, as in the model experiment. In the numerical calculations, two patterns of critical Shields numbers τ_{cr}, 0.03 and 0.05, were considered, with and without considering the suspended sand phenomenon.

Fig. 11 shows the topographic changes in the seabed around cylindrical structures after 2400 wave loads under various conditions. Regardless of the critical Shields parameter or the presence of suspended sand, a decrease in the bed surface due to scouring is observed at the front side of the cylindrical structures (around θ_{cyl} = 45°), while an increase in the bed surface due to deposition is noted at the rear side (around θ_{cyl} = 135°). This topographic change phenomenon is consistent with the trend observed in model experiments (Fig. 9). Fig. 12 presents the temporal changes in the maximum scour depth around the cylindrical structures. The numerical analysis indicates that deeper scour depths tend to occur when accounting for suspended sand phenomena and a smaller critical Shields parameter. Compared with the results from model experiments, the case considering suspended sand phenomena with a critical Shields parameter of 0.03 tended towards similar maximum scour depths after 2400 wave loads. However, the scour depths from the model experiments were greater than those from the numerical analysis. This discrepancy should be analyzed in future work, and a reconsideration of the models for bed load and suspended load sand may be required.

6. CONCLUSION

In this study, numerical simulations using REEF3D were conducted to elucidate the wave-induced transport of sediment around a cylindrical structure, and the reproducibility of the simulation was examined by comparing the results with those from model experiments. The topographic changes observed in the model test were also discussed based on the wave response around the cylindrical structure. The following conclusions were drawn:

- Wave passage tests conducted without the presence of a cylindrical structure exhibited water level and velocity fluctuations that were generally equivalent to the results of the model experiment, indicating good reproducibility.
- Wave response analysis including the cylindrical structure indicated an increased velocity vector from 30° to 135° along the side of the columnar structure, suggesting the occurrence of localized scouring, as observed in the model test. On the other hand, the simulated velocities at 0° (front) and 180° (back) of the column were low, suggesting that sand transport is deposited.
- The comparison between the numerical and model experiment results showed that the case considering suspended sand phenomena with a critical Shields parameter of 0.03 tended towards similar maximum scour depths after 2400 wave loads. However, the scour depths from the model experiments were greater than those from the numerical analysis.

This discrepancy in topographic change phenomena between the numerical and model experiments should be analyzed in future work. Moreover, the models for bed load and suspended load sand in numerical simulation may be revisited.

7. ACKNOWLEDGMENTS

This study was supported by JSPS Grant-in-Aid for Scientific Research (C) 17K06553 and 22K04330, JSPS Grant-in-Aid for Young Scientists 20K14824, Research Foundation for the Electrotechnology of Chubu R-01234 and The Geo-science Center Foundation exclusively in Japan. The authors would like to thank Rikuto Suzuki and FumiyaTakeno who a graduate of the Master's Program at Toyohashi

University of Technology, provided invaluable assistance and help with the model tests.

8. REFERENCES

[1] Sumer B.M., Fredsøe J., Christiansen N., Scour around vertical pile in waves, Journal of Waterway, Port, Coastal, and Ocean Engineering, Vol. 118, No. 1, 1992, pp. 15-31.

[2] Mayall R.O., McAdam R.A., Byrne B.W., Burd H.J., Sheil B.B., Cassie P., Whitehouse R.J.S., Experimental modelling of the effects of scour on offshore wind turbine structures, Proc. of the 9th International Conference Physical Modelling in Geotechnics, 2018, pp. 725-730.

[3] Miyamoto J., Tsurugasaki K., Sassa S., Wave-induced liquefaction and the stability of offshore monopole, Proc. of 9th International Conference of Scour and Erosion, ICSE, 2018, pp. 427-432.

[4] Matsuda T., Miura K., Takayanagi R., Makino R., Wave flume experiment on the scour around cylindrical structure considered to influence effective stress change in the seabed, Proc. of International Conference on Scour and Erosion, ICSE, 2021.

[5] Kamath A., Alagan Chella M., Bihs H., Arntsen Ø.A., CFD Investigations into Wave Forces and Flow around Three Cylinders Placed in Different Configurations, Engineering Applications of Computational Fluid Mechanics, Vol. 9, No. 1, 2015, pp. 343-354, DOI: 10.1080/19942060.2015.1031318.

[6] Ahmad N., Bihs H., Myrhaug D., Kamath A., Arntsen Ø.A., Three-Dimensional Numerical Modelling of Wave-Induced Scour Around Piles in a Side-by-Side Arrangement, Coastal Engineering, Vol. 138, 2018, pp. 132-151, DOI: 10.1016/j.coastaleng.2018.04.016

[7] Dean, R. G., Heuristic models of sand transport in the surf zone, Proc. Conf. Eng. Dynamics in the Surf Zone, 1973, pp. 208-214.

[8] Ahmad N., Kamath A., Bihs H., 3D numerical modelling of scour around a jacket structure with dynamic free surface capturing, Ocean Engineering, 200, 2020, 107104.

[9] van Rijn, L.C., Sediment transport, Part I: Bed load transport. J. Hydraul. Eng., 110 (10), 1984, pp.1431-1456.

[10] Shields, A., Anwendungen der Ähnlichkeitsmechanik und der Turbulenzforschung auf die Geschiebebewegung. Mitteilungen der Preuischen Versuchsanstalt für Wasser-, Erdund Schiffbau, 1936.

[11] Matsuda T., Miura K., Anai K., Sawada Y., Takayanagi R., (2018)., Stress change in seabed induced by sea wave on wave flume experiment in 1g field, Proc. of the 9th International Conference on Scour and Erosion, ICSE 2018, 243-248.